Ultrafine Mo_2C Nanoparticles Embedded in MOF Derived N and P co-doped Carbon Matrix for Efficient Electrocatalytic Oxygen Reduction Reaction in Zinc-Air Batteries

LinYe,[1] Yiran Ying,[1] Dengrong Sun,[1] Jinli Qiao,[2] and Haitao Huang[1*]

1 Department of Applied Physics, The Hong Kong Polytechnic University, Hung Hom, Kowloon, Hong Kong, China

2 College of Environmental Science and Engineering, State Key Laboratory for Modification of Chemical Fibers and Polymer Materials, Donghua University Shanghai 201620, China

E-mail*: aphhuang@polyu.edu.hk*

---

*

1 Experimental

1.1 Materials

2-methylimidazole (MeIM), zinc nitrate ($Zn(NO_3)_2 \cdot 6H_2O$), phosphomolybdic acid ($H_3PMo_{12}O_{40} \cdot nH_2O$, PMo_{12}) and methanol were all used without further purification.

1.2. Preparations

Synthesis of PMo_{12}@ZIF-8. A mixture of $Zn(NO_3)_2 \cdot 6H_2O$ (950mg) in methanol (20 mL) and 3mL of $H_3PMo_{12}O_{40} \cdot nH_2O$ solution (40, 60 and 80 mg PMo_{12} in 10mL deionized water) were vigorously stirred at room temperature for 15 min, and then 2-methylimidazole (2g) in methanol (20 mL) was quickly added, and the resultant mixture became turbid immediately. The solution was aged at room temperature for 24 h. After that, the powders were collected by centrifugation, washed by copious water and methanol to completely remove PMo_{12}, and finally dried overnight at 60 °C in an oven. For comparison, ZIF-8 was also synthesized by a similar method in the absence of $H_3PMo_{12}O_{40} \cdot nH_2O$.

Synthesis of N, P-Doped Mo_2C (Mo_2C@NPC**).** In a typical synthesis, PMo_{12}@ZIF-8 was transferred to a quartz tube to pyrolyze at 950 °C for 3 h with a ramping rate of 5 °C min^{-1} under Ar flow. For comparison, nitrogen doped carbon (C-N) was also synthesized by a similar method in the absence of $H_3PMo_{12}O_{40} \cdot nH_2O$.

1.3. Characterizations

The crystal structure of as-prepared samples were carried out by a Bruker D8 ADVANCE X-ray diffraction with Cu Kα radiation (λ=0.15418 nm), which was operated at 40 kV and 40mA. The morphology of the samples was obtained by a field emission scanning electron microscopy (FE-SEM) (JSM-6700F). The transmission electron microscopy (TEM) and high resolution transmission electron microscopy (HRTEM) images were obtained in a JEOL model JEM 2010 EX instrument at an accelerating voltage of 200 kV. The powder particles were supported on a carbon film coated on a 3-mm-diameter fine mesh copper grid. The sample suspension was sonicated in ethanol and a drop of it was dripped on the copper grid. X-ray photoelectron spectra (XPS) was characterized by a Thermo Scientific ESCA Lab 250 system, with a monochromatic Al Kα as the X-ray source and a hemispherical analyzer. For BET surface area analyses, the samples were degassed in vacuum at 120 °C for 10 h and then measured at 77 K. The Raman spectroscopy was performed using an invia-Reflex Micro-Raman Spectroscopy system (Renishaw Co.) with 532 nm line of an Ar ion laser at room temperature. Electrochemical properties were measured on an electrochemical analyzer (CHI760). Thermal gravity (TG) analysis was obtained by using a Hitachi HT-Seiko Instrument Exter 6300 TG/DTA. Fourier transform infrared spectroscopy (FTIR) measurements were recorded on a thermoscientific Nicolet 4700 using KBr pellets. Inductively coupled plasma optical emission spectroscopy (ICP-OES) was used to examine the content of Mo element by using a Hitachi model SPS3520UV-DD. The Elemental Analyzer was employed to determine the elemental composition.

1.4. Electrochemical measurements.

Sample preparation. 5mg of ORR catalyst was dispersed into H_2O (420μL) and anhydrous ethanol (30 μL), then Nafion solution (50 μL) was added, followed by mixing with the assistance of ultrasonication for at least 30 min to achieve a homogeneous ink. Next, 6 μL of the catalyst ink was pipetted onto a glassy carbon electrode (d=3 mm, S=0.07 cm^2). Commercial 20 wt% platinum on carbon black (Pt/C, BASF) was measured for comparison, where 5 mg Pt/C was dispersed in 1 mL Nafion solution (0.25 wt %) by sonication for more than 1h to obtain a well-dispersed ink and then 6 μL of the catalyst ink was pipetted onto the glassy carbon electrode surface.

ORR performance tests. All the electrochemical measurements were carried out in a conventional three-electrode cell using a CHI660E electrochemical workstation (Shanghai Chenhua Instrument Co., China) at room temperature. The glassy-carbon (GC) rotating ring disk electrode (RRDE) (diameter 3 mm, area 0.07065 cm^2), the Pt wire and Ag/AgCl electrode (with saturated KCl solution) were used as working, counter, and reference electrodes, respectively. All the potentials in this study were calibrated with a reversible hydrogen electrode (RHE), with the potential conversion formula as, $E_{RHE} = E_{Ag/AgCl} + 0.0591\ V \times pH$ (at 25 °C).

Calculation of the electron transfer number (n). The Koutecky-Levich plot presents the relationship of J^{-1} versus $\omega^{-1/2}$ and the Koutecky-Levich equation is shown below:

$$\frac{1}{|J|} = \frac{1}{|J_L|} + \frac{1}{|J_K|} = \frac{1}{B\sqrt{\omega}} + \frac{1}{|J_K|}$$

$$B = 0.2nFC_0(D_0)^{2/3}\upsilon^{-1/6}$$

where J, J_L and J_K are the measured, diffusion limiting, and the kinetic-limiting current densities, respectively; ω is the rotation speed in rpm, F is the Faraday constant (96,485 C mol-1), C_0 is the bulk concentration of oxygen (1.2×10^{-6} mol·cm^{-1}), D_0 is the diffusion coefficient of oxygen in 0.1 M KOH (1.9×10^{-5} cm^2·s^{-1}), and υ is the kinetic viscosity (0.01 cm^2·s^{-1}). The n can be calculated from the slope of the K-L plot.

The electron transfer number (n) can be also calculated based on RRDE measurements as the following equation:

$$n = \frac{4I_D}{I_D + \frac{I_R}{N}}$$

where I_D is the disk current, I_R is the ring current, and N is the current collection efficiency of the Pt ring.

The ratio of the H_2O_2 production can be calculated by (I_0/I)*100%. I_0 represents the current density.

Zinc-air batteries assembly and measurement. To prepare zinc-air batteries, the prepared catalysts powder was ultrasonically dispersed in a 1mL mixed solution (the volume ratio of DI-water, 0.05wt% Nafion and ethanol was 6 : 1 : 3) for 30 min to form a concentration of 10 mg/mL catalyst ink. Then the ink was coated onto carbon paper and dried under a lamp. The loading mass density was about 1mg cm^{-2}. A piece of Zinc plate was used as anode electrode and 6 M KOH was used as electrolyte. The zinc-air batteries were tested at room temperature. The polarization curves were obtained by LSV technique with CHI760E electrochemical work station. The galvanostatic discharge and charge cyclings were performed in LAND testing system. The specific capacity of zinc-air batteries was calculated from the following equation:

$$C_{sp} = \frac{i \times t}{\triangle m}$$

where i is discharge current, t is discharge time and $\triangle m$ is the weight of consumed zinc.

Computational Details

All density functional theory (DFT) calculations were performed in the VASP package by using the projector-augmented wave method.[1-2] Perdew-Burke-Ernzerhof generalized gradient approximation was used for the exchange-correlation functional.[3] Kinetic energy cut-off was set as 450 eV, and energy and force convergence criteria were set as 10^{-5} eV and 0.02 eV/Å, respectively. The van der Waals corrections were considered by the DFT-D3 scheme.[4] The Brillouin zone was sampled by Gamma-centered 3×3×1 k-points meshes. A vacuum layer (15 Å) was added to avoid interactions between adjacent layers. The initial structure of C-N was modeled by a 6×6 graphene lattice doped with one N atom. Computational hydrogen electrode (CHE) model was used in the calculations, and Gibbs free energy changes ΔG were calculated as $\Delta G = \Delta E + \Delta ZPE – T\Delta S + \Delta G_U$, where ΔE, ΔZPE, and $T\Delta S$ represent changes in DFT-calculated energy, zero-point energy, and entropy contribution (T was set as 298 K), respectively, and $\Delta G_U = -neU$ (U is the applied potential and n is the number of transferred proton-electron couples).[5] The solvation effect was considered by adding a -0.3 eV correction to the calculated ΔG of *OH and *OOH.[6]

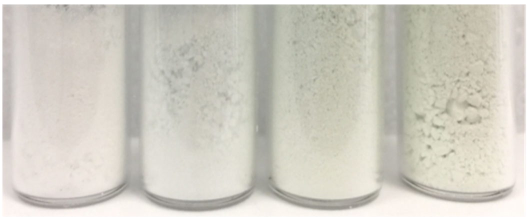

Fig. S1 The color change of the Mo_2C@NPC-*x* which is derived from PMo_{12}@ZIF-8-*x*.

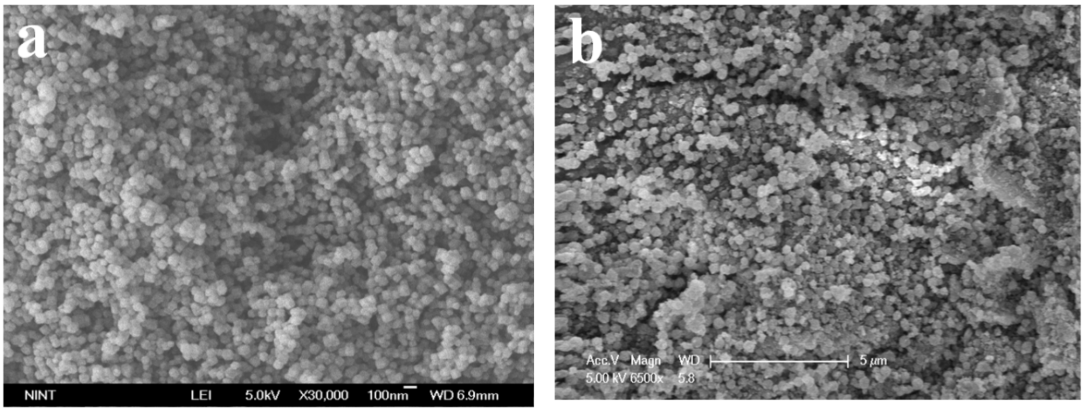

Fig. S2 SEM images of (a) ZIF-8, and (b) PMo_{12}@ZIF-8.

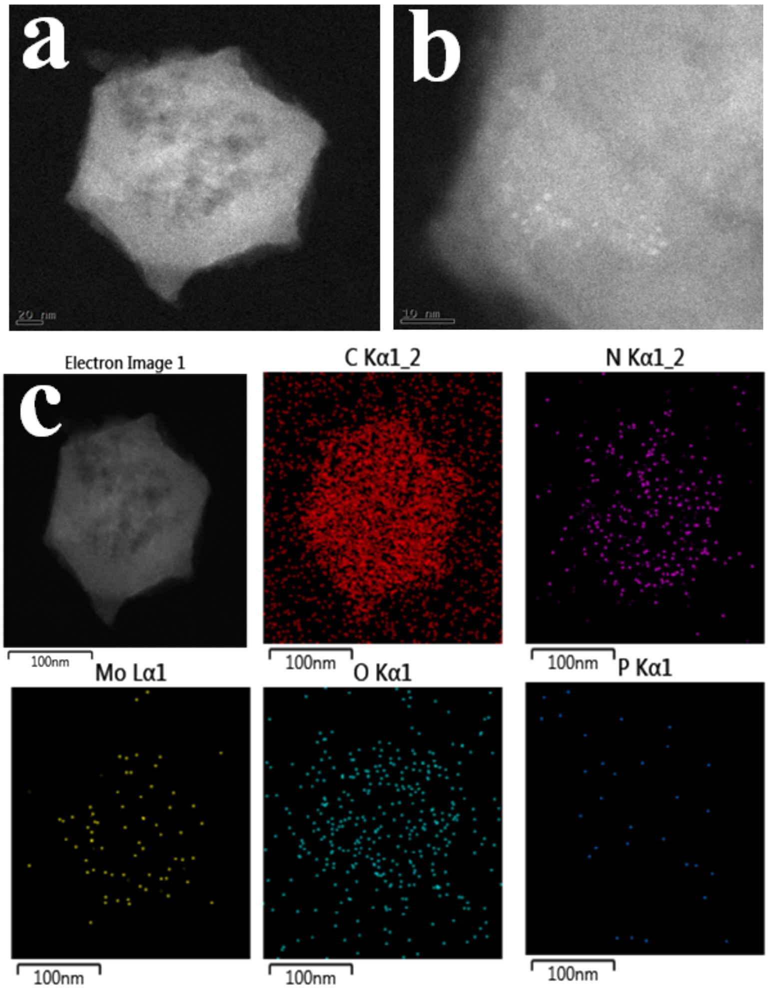

Fig. S3 (a-b) TEM, (c) STEM-EDS elemental mappings of C, N, P, O and Mo of Mo_2C@NPC-1.2.

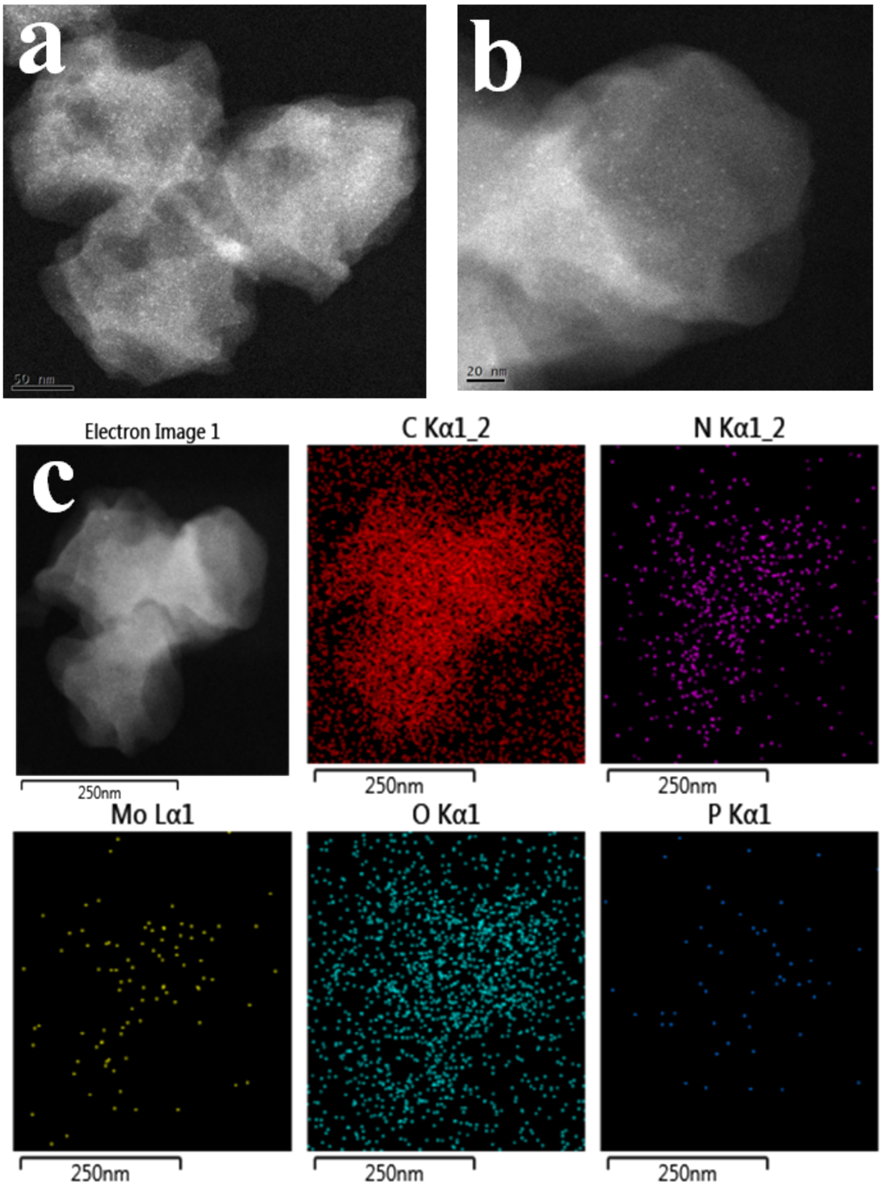

Fig. S4 (a-b) TEM, (c) STEM-EDS elemental mappings of C, N, P, O and Mo of Mo_2C@NPC-3.4.

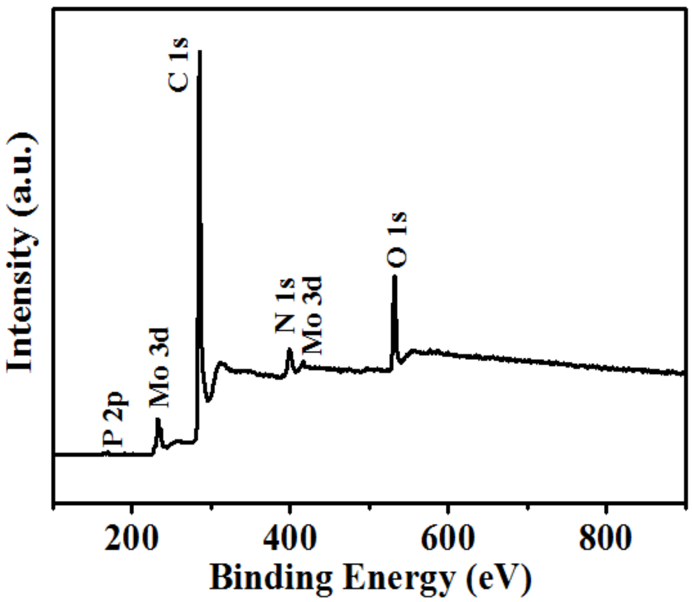

Fig. S5 The XPS survey spectrum of Mo_2C@NPC-2.6.

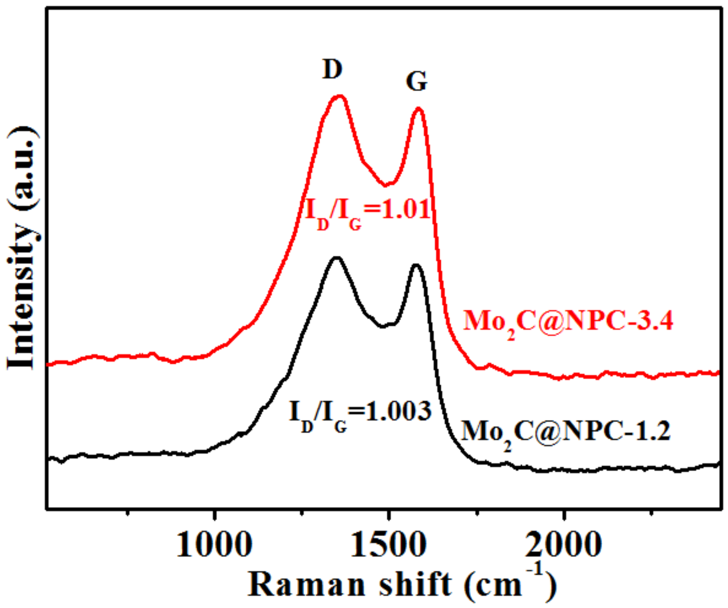

Fig. S6 Raman spectra of Mo_2C@NPC-1.2 and Mo_2C@NPC-3.4.

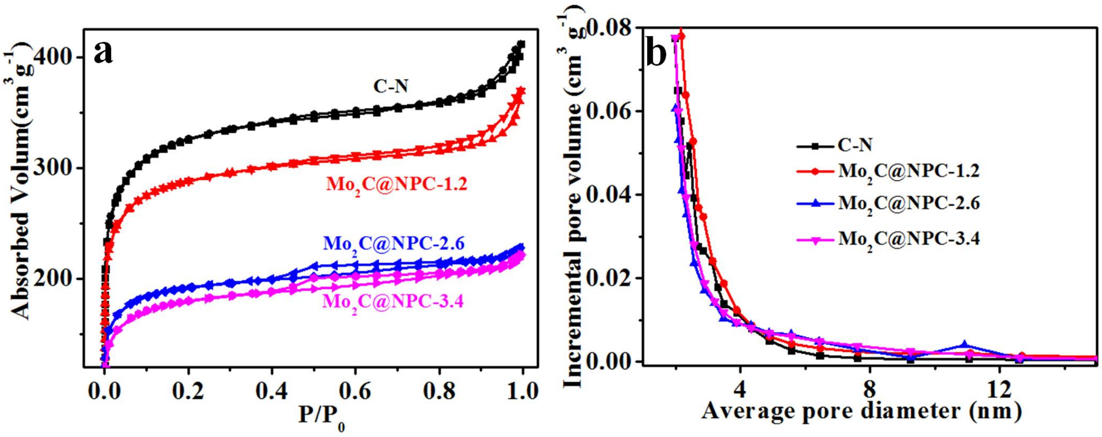

Fig. S7 (a) N_2 adsorption-desorption isotherms, and (b) pore size distribution of C-N and Mo_2C@NPC-*x*.

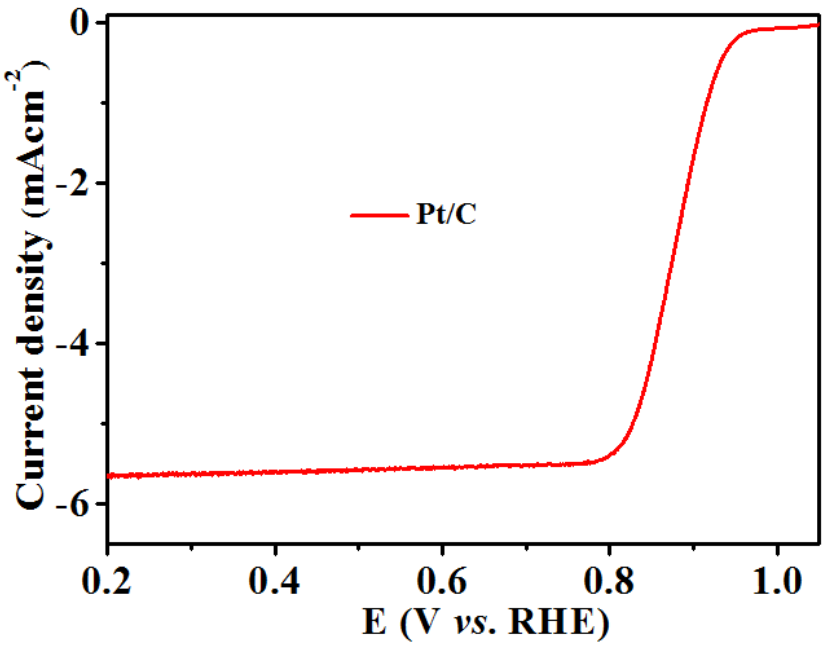

Fig. S8 ORR polarization plots for Pt/C catalyst at the rotation speed of 1600 rpm.

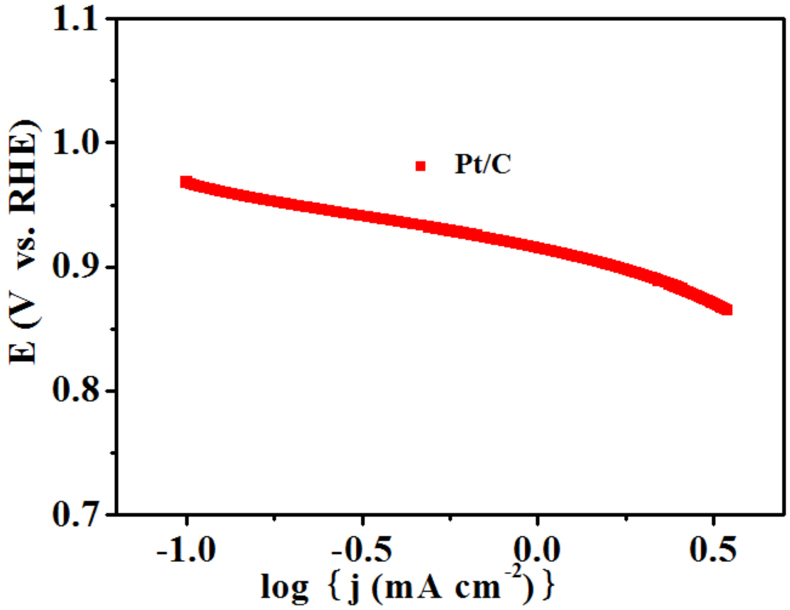

Fig. S9 Corresponding Tafel slope extracted from RRDE curves of Pt/C catalyst.

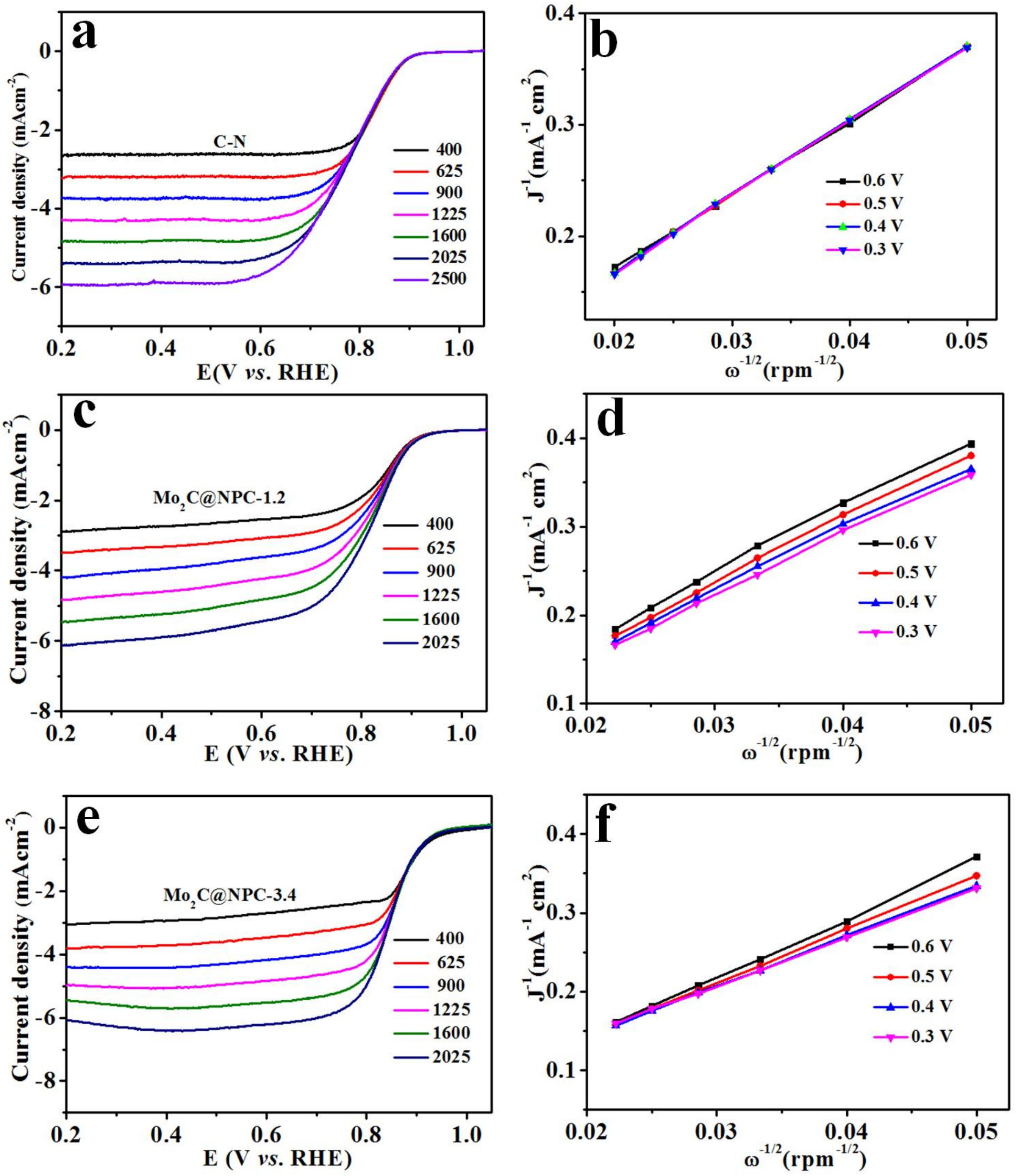

Fig. S10 (a, c, e) LSV curves of Mo_2C@NPC-*x* and C-N at different rotation speeds, and (b, d, f) Corresponding Kouteck-Levich plots derived from the RDE data of Mo_2C@NPC-*x* and C-N.

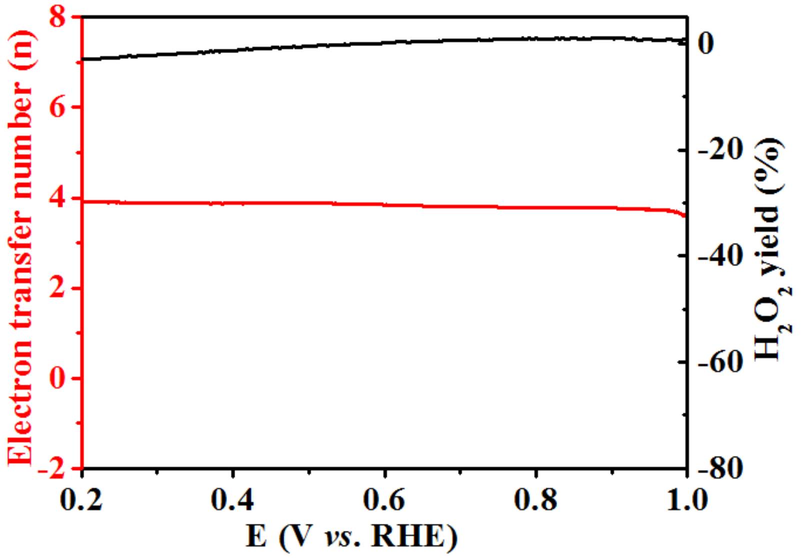

Fig. S11 Peroxide yield and electron transfer number of Mo_2C@NPC-2.6 at various potentials from RRDE.

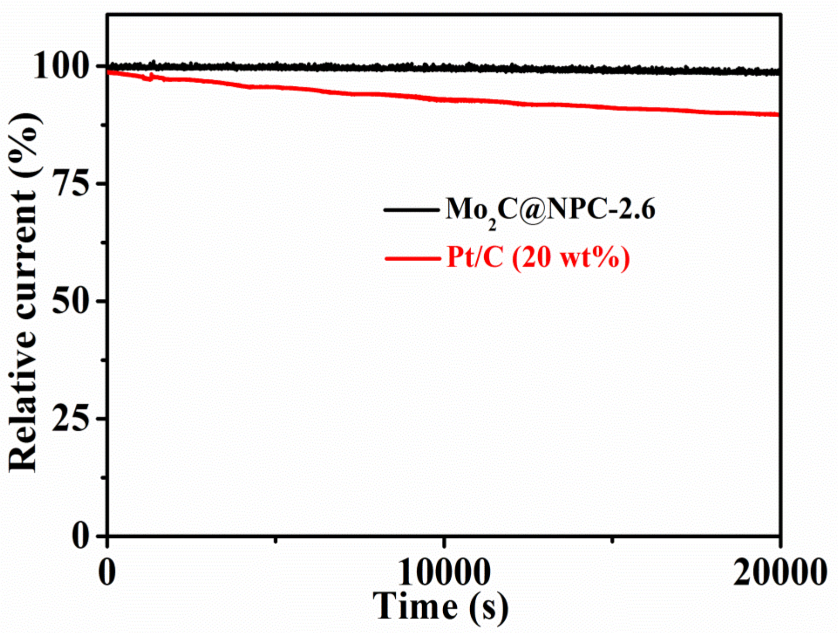

Fig. S12 I-t chronoamperometric response of Mo_2C@NPC-2.6 and bench-mark Pt/C electrodes in O_2-saturated 0.1 M buffer solution at a rotation speed of 1600 rpm.

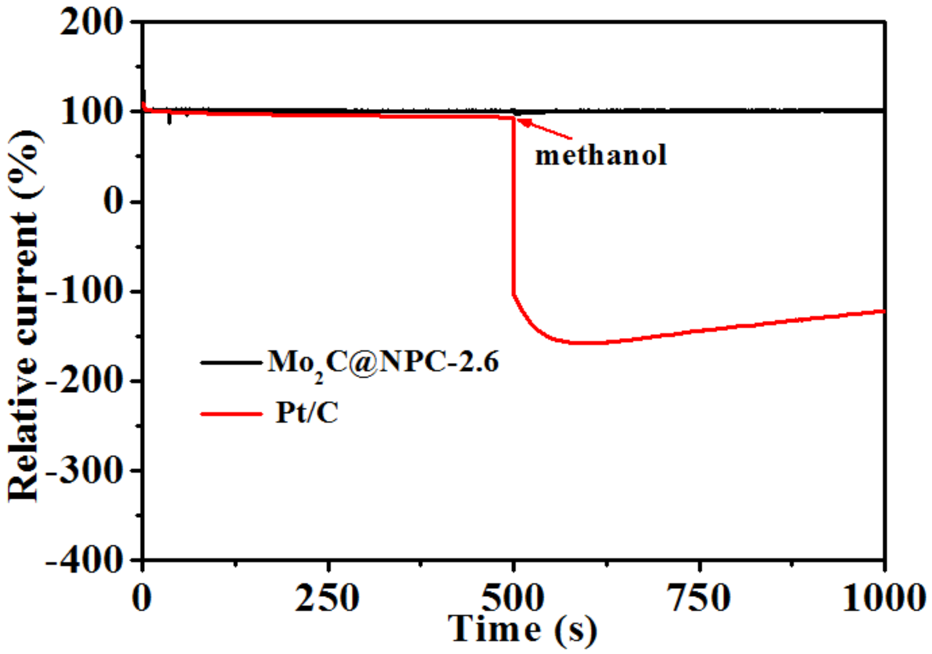

Fig. S13 Current-time (I-t) curves for Mo$_2$C@NPC-2.6 and Pt/C in O_2-saturated 0.1 M KOH solution with 2 M CH_3OH added at around 500 s.

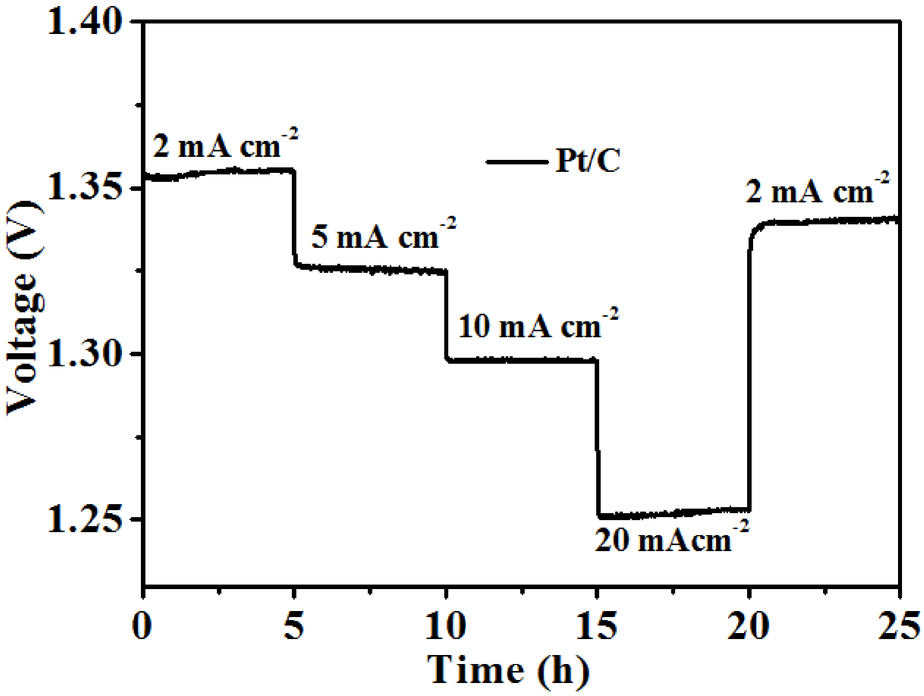

Fig. S14 Discharge curves of the primary Zinc-air batteries using Mo_2C@NPC-2.6 as the cathode catalyst at various current densities.

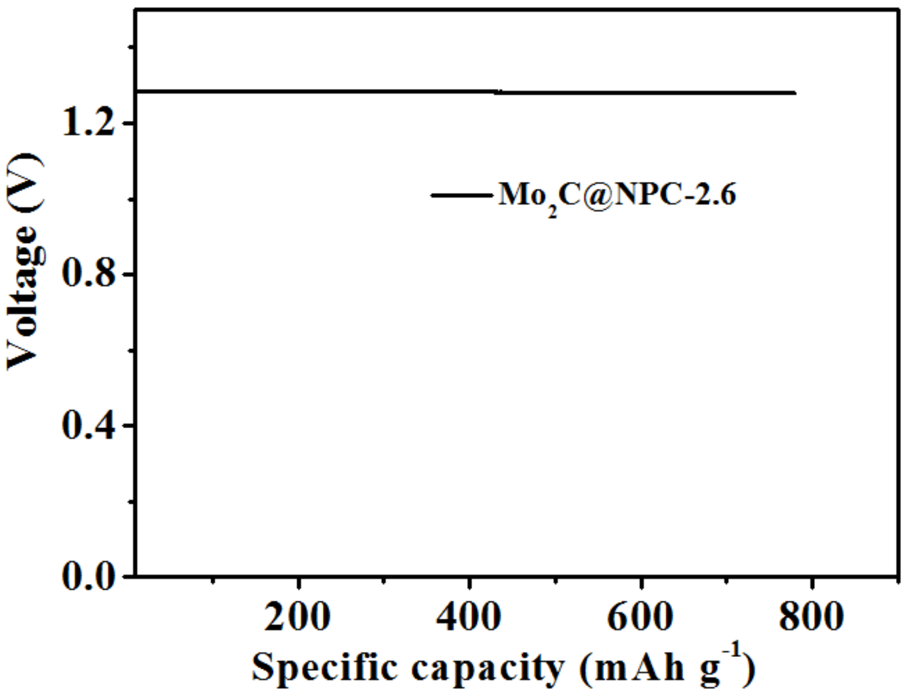

Fig. S15 The specific capacity of the primary Zn-air batteries using Mo_2C@NPC-2.6 as the cathode catalysts.

Catalyst	**Mo(%)**	**N(%)**	**P(%)**
C-N	0	1.15	0
Mo_2C@NPC-1.2	1.2	1.23	0.034
Mo_2C@NPC-2.6	2.6	1.89	0.064
Mo_2C@NPC-3.4	3.4	2.56	0.084

Table S1 The amount of the Mo, N and P in C-N and Mo_2C@NPC-*x*.

Catalyst	**Onset potential (V)**	**Half-wave potential (V)**	**Diffusion limited current $mAcm^{-2}$**	**Reference**
Mo_2C@NPC-2.6	**1.01**	**0.90**	**5.63**	**This work**
Mo_2C/NPCNFs	0.9	0.77	4.6	7
FeMo Carbide/NG	0.912	-	3.5	8
Mo_2C-C-5	0.832	0.713	5.52	9
Mo_2C@NC	1.0	0.872	3.9	10
Mo_2C-GNR	0.93	0.8	4.6	11
Co-N-MoO_2	0.87	~0.81	3.2	12
MoC/NGr-3	0.93	0.8	6.0	13
Co-Mo-ON/NG	0.915	0.835	~3.82	14
Co-N/CNFs	0.92	0.82	5.2	15
7.1%Cu-Co_2P@NPC	0.95	0.835	5.2	16
GL-Fe/Fe_5C_2/NG/800	0.98	0.86	-	17
Cu@Fe-N-C/900	1.01	0.892	5.5	18
Fe-SA/PC	-	0.91	5.4	19
NSHPC	1.04	0.89	5.45	20
Co-ISAS/p-CN	~0.90	0.838	~5.2	21
Fe_2-Z8-C	0.985	0.871	-	22

Table S2 Comparison of the ORR performance for Mo_2C@NPC-2.6 and some representative transition metal catalysts recently reported in 0.1 M KOH solution.

Catalyst	**Catalyst loading ($mg\ cm^{-2}$)**	**Maximum power density ($mW\ cm^{-2}$)**	**Reference**
Mo_2C@NPC-2.6	**1**	**266**	**This work**
3DOM Fe-N-C-900	1	235	23
c-CoACC/CNTs	1	188	24
7.1%Cu-Co_2P@NPC	1	236.1	16
Co_2P/CoN-in-NCNTs	0.5	194.6	25
$Pb_2Ru_2O_{6.5}$	0.85	195	26
Fe@N-C-700	2.2	220	27
Fe-SAs/NPS-HC	1	195.0	28
FeN_x-PNC	0.2	278	29
NCo@CNT-NF700	0.5	220	30
$CoFe_{20}$@CC	0.52	190.3	31
Co_4N@NC	1	74.3	32

Table S3 The performance of recently reported zinc-air batteries with nonprecious catalysts.

Reference

[1] G. Kresse, J. Furthmüller, *Phys. Rev. B*, 1996, **54**, 11169.

[2] G. Kresse, D. Joubert, *Phys. Rev. B*, 1999, **59**, 1758.

[3] J. P. Perdew, K. Burke, M. Ernzerhof, *Phys. Rev. Lett.,* 1996, **77**, 3865.

[4] S. Grimme, J. Antony, S. Ehrlich, H. Krieg, *J. Chem. Phys.,*2010, **132**, 154104.

[5] J. K. Nørskov, J. Rossmeisl, A. Logadottir, L. Lindqvist, J. R. Kitchin, T. Bligaard, H. Jonsson, *J. Phys. Chem. B*, 2004, **108**, 17886-17892.

[6] H. Xu, D. Cheng, D. Cao, X. C. Zeng, *Nat. Catal.*, 2018, **1**, 339-348.

[7] H. Wang, C. Sun, Y. J. Cao, J. T. Zhu, Y. Chen, J. Guo, J. Zhao, Y. H. Sun and G. F. Zou, *Carbon*, 2017, **114**, 628-634.

[8] M. H. Chen, J. L. Liu, W. J. Zhou, J. Y. Lin and Z. X. Shen, *Sci. Rep.*, 2015, **5**, 10389.

[9] Y. Luo, Z. J. Wang, Y. Fu, C. Jin, Q. Wei and R. Z. Yang, *J. Mater. Chem. A*, 2016, **4**, 12583.

[10] Z. H. Cheng, Q. Fu, Q. Han, Y. K. Xiao, Y. Liang, Y. Zhao and L. T. Qu, *Adv. Funct. Mater.*, 2018, **28**, 1705967.

[11] X. Fan, Y. Liu, Z. Peng, Z. Zhang, H. Zhou, X. Zhang, B. I. Yakobson, W. A. Goddard III, X. Guo, R. H. Hauge and J. M. Tour, *ACS Nano*, 2017, **11**, 384-394.

[12] H. Huang, C. Du, S. Wu and W. Song, *J. Phys. Chem. C*, 2016, **120**, 15707-15713.

[13] L. Yang, J. Yu, Z. Wei, G. Li, L. Cao, W. Zhou, S. Chen, *Nano Energy*, 2017, **41**, 772-779.

[14] K. Sharma, D. Hui, N. H. Kim and J. H. Lee, Nanoscale, 2019, **11**, 1205.

[15] Q. Q. Cheng, L. J. Yang, L. L. Zou, Z. Q. Zou, C. Chen, Z. Hu, H. Yang, *ACS Catal.*, 2017, **7**, 6864-6871.

[16] L. C. Diao, T. Yang, B. Chen, B. Zhang, N. Q. Zhao, C. S. Shi, E .Z. Liu, L. Y. Ma and C. N. He, *J. Mater. Chem. A*, 2019, **7**, 21232.

[17] E. Hu, X. Y. Yu, F. Chen, Y. Wu, Y. Hu and X. W. D. Lou, *Adv. Energy Mater.*, 2018, **8**, 1702476.

[18] Z. H. Wang, H. H. Jin, T. Meng, K. Liao, W. Q. Meng, J. L. Yang, D. P. He, Y. L. Xiong and S. C Mu, Fe, *Adv. Funct. Mater.*, 2018, **28**, 1802596.

[19] J. J. Huo, L. Lu, Z. Y. Shen, Y. Liu, J. J. Guo, Q. B. Liu, Y. Wang, H. Liu, M. H. Wu and G. X. Wang, *J. Mater. Chem. A*, 2020, **8**, 16271.

[20] R. R. Li, F. Liu, Y. H. Zhang, M. M. Guo and D. Liu, *ACS Appl. Mater. Interfaces*, 2020, **40**, 44578-44587.

[21] A. J. Han, W. X. Chen, S. L. Zhang, M. L. Zhang,Y. H. Han, J. Zhang, S. F. Ji, L. R Zheng, Y. Wang, L. Gu, C. Chen, Q. Peng, D. S. Wang and Y. D. Li, *Adv. Mater.*, 2018, **30**, 1706508.

[22] Q. T. Liu, X. F. Liu, L. R. Zheng and J. L. Shui, *Angew. Chem. Int. Ed.*, 2018, **57**, 1204.

[23] X. B. Zhang, X. Han, Z. Jiang, J. Xu, L. N. Chen, Y. K. Xue, A. M. Nie, Z. X. Xie, Q. Kuang and L. S. Zheng, *Nano Energy*, 2020, **71**, 104547.

[24] Y. P. Li, S. Q. Ci, P. W. Cai, N. Senthilkumar and Z. H. Wen, *Electrochim. Acta*, 2020, **353**, 136605.

[25] Y. Guo, P. Yuan, J. Zhang, H. Xia, F. Cheng, M. Zhou, J. Li, Y. Qiao, S. Mu and Q. Xu, *Adv. Funct. Mater.*, 2018, **28**, 1805641.

[26] C. Duan, D. Hook, Y. Chen, J. Tong and R. OHayre, *Energy Environ. Sci.*, 2017, **10**, 176-182.

[27] J. Wang, H. H. Wu, D. F. Gao, S. Miao, G. X. Wang and X. H. Bao, *Nano Energy*, 2015, **13**, 387-396.

[28] Y. J. Chen, S. F. Ji, S. Zhao, W. X. Chen, J. C. Dong, W. C. Cheong, R. Shen, X. D. Wen, L. R. Zheng, A. I. Rykov, S. C. Cai, H. L. Tang, Z. B. Zhuang, C. Chen, Q. Peng, D. S. Wang and Y. D. Li, *Nat. Commun.*, 2018, **9**, 5422.

[29] L. T. Ma, S. M. Chen, Z. X. Pei, Y. Huang, G. J. Liang, F. N. Mo, Q. Yang, J. Su, Y. H. Gao, J. A. Zapien and C. Y. Zhi, *ACS Nano.*, 2018, **12**, 1949-1958.

[30] L. L. Zou, C. C. Hou, Z. Liu, H. Pang and Q. Xu, *J. Am. Chem. Soc.*, 2018, **140,** 15393.

[31] C. C. Hou , L. L. Zou, Q. Xu, *Adv. Mater.*, 2019, **3**, 1904689.

[32] H. Y. Ge, G. D. Li, J. X. Shen, W. Q. Ma, X. G. Meng and L. Q. Xu, *Appl. Catal. B: Environ.*, 2020, **275**, 119104.